Accepted Manuscript

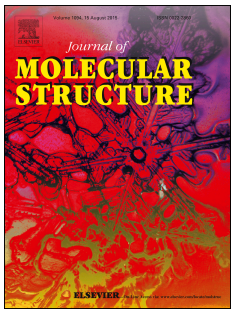

Synthesis, quantum chemical, in vitro acetyl cholinesterase inhibition and molecular docking studies of four new coumarin based pyrazolylthiazole nuclei

Murtaza Madni, Muhammad Naeem Ahmed, Shahid Hameed, Syed Wadood Ali Shah, Umer Rashid, Khurshid Ayub, M.Nawaz Tahir, Tariq Mahmood

PII: S0022-2860(18)30573-8

DOI: 10.1016/j.molstruc.2018.05.017

Reference: MOLSTR 25189

To appear in: *Journal of Molecular Structure*

Received Date: 18 November 2017

Revised Date: 9 April 2018

Accepted Date: 6 May 2018

Please cite this article as: M. Madni, M.N. Ahmed, S. Hameed, S.W. Ali Shah, U. Rashid, K. Ayub, M.N. Tahir, T. Mahmood, Synthesis, quantum chemical, in vitro acetyl cholinesterase inhibition and molecular docking studies of four new coumarin based pyrazolylthiazole nuclei, *Journal of Molecular Structure* (2018), doi: 10.1016/j.molstruc.2018.05.017.

Graphical abstract

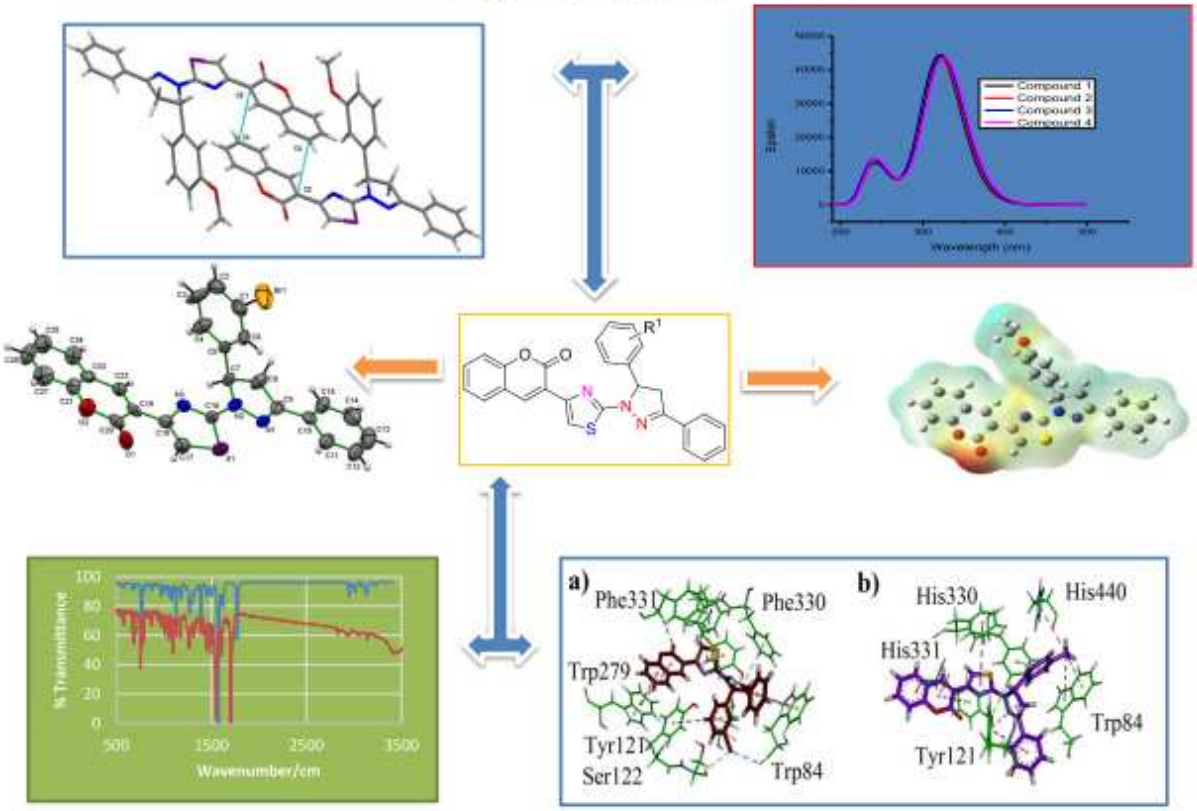

Synthesis, quantum chemical, *in vitro* acetyl cholinesterase inhibition and molecular docking studies of four new coumarin based pyrazolylthiazole nuclei

Murtaza Madni[a], Muhammad Naeem Ahmed [b], Shahid Hameed [a*], Syed Wadood Ali Shah [c], Umer Rashid [d], Khurshid Ayub [d], M. Nawaz Tahir [e], Tariq Mahmood [d*]

[a] Department of Chemistry, Quaid-i-Azam University, Islamabad 45320, Pakistan.

[b] Department of Chemistry, The University of Azad Jammu and Kashmir Muzaffarabad, 13100 Pakistan.

[c] Department of Pharmacy, University of Malakand, KPK, Pakistan.

[d] Department of Chemistry, COMSATS Institute of Information Technology, University Road, Tobe Camp, 22060, Abbottabad, Pakistan.

[e] Department of Physics, University of Sargodha, Sargodha, Pakistan.

*To whom correspondence should be addressed: E-mail: mahmood@ciit.net.pk (T. M) and shameed@qau.edu.pk (S. H).

Abstract

Four new *3-(2-(3-Phenyl-5-substituted phenyl-4,5-dihydropyrazol-1-yl)thiazol-4-yl)-2H-chromen-2-one* derivatives (**1-4)** were synthesized and fully characterized by spectroscopic techniques. The final structures of all chromenone analogues (**1-4**) were confirmed by single crystal X-ray diffraction analysis. Quantum chemical studies were performed to compare the results from the theoretical studies with the experimental (X-ray as well as spectroscopic) ones. The theoretically simulated geometric parameters and other spectroscopic properties agreed nicely with the experimental data. All compounds were evaluated for biological activity (acetyl cholinesterase inhibition potential). Compound **3** emerged as the most potent derivative in acetylcholine esterase (AChE) inhibition assay with IC_{50}=27.29 µM. The IC_{50} of compound **3** is greater than the standard drug galantamine (IC_{50}=44.02 µM). To rationalize the potencies, molecular docking studies were also carried out. These docking results revealed a good correlation between binding energies values and in vitro AChE inhibition assay.

Keywords: Coumarin; X-ray; DFT; Acetyl cholinesterase; Molecular docking

1. Introduction

Thiazole scaffold is a basic unit of a large number of natural and synthetic molecules having wide spread biological applications. The famous reported biological applications of thiazole containing molecules include antibacterial, antifungal, antiviral, anticancer, antiparkinsonian, and anti-inflammatory activities [1–4]. The importance of the thiazole moiety is also reflected by its presence in large number of marketed drugs as an active group [5]. Besides thiazole, pyrazole is also a biologically important structural motif. Several cyclooxygenase-2 (COX-2) inhibitors possess pyrazole and pyrazoline nuclei as key moieties in their chemical structures [6–8]. In literature, many pyrazoline containing compounds e.g. mefobutazone, kebuzone, phenylbutazone [9] and ramifenazone [10] are reported to have potent anti-inflammatory activity.

The importance of coumarin moiety is very well reflected by its presence in many antibiotics. Moreover antibacterial activity of coumarins against Gram-positive bacteria is also reported in the literature [11–13]. Dicoumarol and warfarin contain coumarin moiety and are used as anticoagulant of blood in different organs (veins, lungs and heart) of living beings [14]. Apart from the pharmacological properties, substituted coumarin derivatives also find applications in dyes due to their unique optical and photophysical properties [15]. Coumarin-thiazoles based dyes are used as fluorescence labels [16,17], optical brighteners [18,19], non-linear optical materials [20], solar energy absorbers, laser dyes and as two-photon absorption (TPA) materials [21]. 3-Substituted pyrazolyl thiazolyl based coumarin dyes have also been used as fluorescent brightening agents [22], red, green and blue dopants in organic light-emitting diodes (OLEDs) [23,24].

Neurodegenerative diseases (NDs) in developed countries are becoming big threat to the general population. The researchers are struggling for pharmacological cures of NDs [25]. Alzheimer's

disease (AD), the common form of dementia, is one of the neurodegenerative diseases (NDs). Some of the major effects of AD include confusion, petulance, memory loss, anger and the absence of potency in body [26]. During the last decade, treatment plan for AD has been focused on the improvement of cholinergic neurotransmission in the brain, which is based on the 'cholinergic hypothesis'. According to this hypothsis, one of the rational and operative methods to treat the AD disease is to raise the acetylcholine (ACh) level through inhibition of acetylcholinesterase (AChE) [26,27]. A few compounds (medicine) for increasing acetylcholine levels in the brain include tacrine, donepezil, rivastigmine and galantamine [28]. The central cholinergic pathways have vital role in memory processes and their damage can be reduced by the improvement of acetylcholine (Ach) levels in brain through AChE inhibitors [29,30]. Synthetic organic compounds with neurobiological action may be possible targets for drug discovery, in this regard [31,32]. Recently, medicinally important coumarin derivatives bearing heterocyclic rings e.g. thiazole, pyrazolyl and thiazole have been reported in literature, in this regard [33–36]. Keeping in view the importance of pyrazolyl and coumarin moieties as useful materials in drug research and in continuation of our previous work on pyrazolylthiazole derivatives [37] and density functional theory investigations of organic compounds [38–41], herein we report the synthesis, structural properties, density functional theory (DFT) studies, acetylcholineesterase inhibition and molecular docking studies of four new coumarin based pyrazolylthiazole derivatives.

2. Material and methods

2.1 Experimental

Substituted benzaldehydes, acetophenone, salicyaldehyde and ethyl acetoacetate were purchased from Sigma-Aldrich and Fluka. The reactions were performed in 100 mL 2-neck round bottom flask having teflon stirring bar, and the progress of the reaction was monitored through thin layer chromatography (TLC). The melting points were determined on a Yanaco melting point apparatus and are reported as uncorrected. FT-IR spectra of all four derivatives were recorded on a Nicolet FT-IR 5DX spectrophotometer. ^{1}H and ^{13}C-NMR spectra were scanned on a JEOL-ECA in $CDCl_3$ with proton and carbon resonances at 400 and 100 MHz, respectively. TMS was used as an internal standard and *J* values are reported in Hz.

2.2 Synthesis

The synthesis of compounds (**1**-**4**) was achieved by following the synthetic scheme provided in Fig. 1.

2.2.1 General Procedure for the synthesis,of coumarin based pyrazolylthiazole nuclei (**1**-**4**)

According to the reported literature procedure [42], acetophenone and appropriate benzaldehydes were condensed to their respective substituted chalcones by treating them with 60% KOH in ethanol. In the next step, 3-Phenyl-5-substituted phenyl-4,5-dihydropyrazole-1-carbothioamide were synthesized by reacting substituted chalcones with thiosemicarbazide [43]. Finally, substituted 3,5-diphenyl-4,5-dihydropyrazole-1-carbothioamides (2 mmol) was added to a suspension of 3-(2-bromoacetyl)-2*H*-chromen-2-one (2 mmol) in ethanol (10 mL). The resultant mixture was stirred vigorously under reflux for 2 hours at room temperature. Then, the reaction

mixture was poured in ice cold water. Precipitates were filtered and recrystallized from chloroform:ethanol (3:1) mixture to afford excellent yields of desired compounds.

2.2.1.1 3-(2-(5-(3-Bromophenyl)-3-phenyl-4,5-dihydropyrazol-1-yl)thiazol-4-yl)-2H-chromen-2-one (**1**).

Pale yellow solid; m.p. 230 °C, yield = 85%, **FT-IR** (ATR, cm^{-1}): ν_{max} 3123, 1709, 1606, 1545, 1485, 1443, 1316, 1247, 1172, 1132, 1087, 962, 752; ^{1}H-NMR (400 MHz, $CDCl_3$): δ 3.38 (1H, dd, J_{cis} = 7.5Hz, $J_{gem.}$ = 17.4Hz, CH pyrazoline), 3.95 (1H, dd, J_{trans} = 12Hz, J_{gem} = 17.4Hz, CH-pyrazoline), 5.54 (1H, dd, J_{cis} = 7.5Hz, J_{trans} = 12Hz, CH-pyrazoline), 7.25-7.85 (14H, m, Ar), 8.19 (1H, s, CH-thiazole); ^{13}C-NMR (100 MHz, $CDCl_3$): δ 43.4, 64.4, 111.8, 116.2, 119.7, 121.2, 122.4, 124.4, 125.0, 126.4, 128.3, 128.7, 130.0, 130.5, 130.7, 130.9, 131.0, 131.0, 138.6, 144.0, 144.3, 151.8, 152.7, 159.7, 164.0.

2.2.1.2 3-(2-(5-(3-Methoxyphenyl)-3-phenyl-4,5-dihydropyrazol-1-yl)thiazol-4-yl)-2H-chromen-2-one **(2)**.

Pale yellow solid, m.p. 265-266 °C, yield = 87%, **FT-IR** (ATR, cm^{-1}): ν_{max} 3145, 1705, 1603, 1554, 1487, 1380, 1317, 1265, 1134, 1053, 1010, 751; ^{1}H-NMR (400 MHz, $CDCl_3$): δ 3.38 (1H, dd, J_{cis} = 7.5Hz, J_{gem} = 17.4Hz, CH-pyrazoline), 3.83 (3H, s, OCH_3), 3.93 (1H, dd, J_{trans} = 12Hz, J_{gem} = 17.4Hz, CH-pyrazoline), 5.59 (1H, dd, J_{cis} = 7.5Hz, J_{trans} = 12Hz, CH-pyrazoline), 6.84-7.83 (14H, m, Ar), 8.23 (1H, s, CH-thiazole); ^{13}C-NMR (100 MHz, $CDCl_3$): δ 43.5, 55.3, 64.9, 111.6, 112.8, 116.2, 118.8, 119.7, 121.2, 124.3, 126.4, 128.1, 128.7, 129.8, 129.9, 130.9, 131.3, 138.6, 143.3, 144.3, 151.9, 152.7, 159.7, 159.8, 164.1.

2.2.1.3 3-(2-(3-Phenyl-5-p-tolyl-4,5-dihydropyrazol-1-yl)thiazol-4-yl)-2H-chromen-2-one **(3)**.

Pale yellow solid, m.p. 250 °C, yield = 88%, **FT-IR** (ATR, cm^{-1}): ν_{max} 3141, 1718, 1550, 1390, 1249, 1174, 1134, 1043, 1005, 752; ^{1}H-NMR (400 MHz, $CDCl_3$): δ 3.32 (3H, s, CH_3), 3.36 (1H, dd, J_{cis} = 7.2Hz, J_{gem} = 17.4Hz, CH-pyrazoline), 3.92 (1H, dd, J_{trans} = 12Hz, J_{gem} = 17.4Hz, CH-pyrazoline), 5.61 (1H, dd, J_{cis} = 7.2Hz, J_{trans} = 12Hz, CH-pyrazoline), 7.19-7.82 (14H, m, Ar), 8.24 (1H, s, CH-thiazole); ^{13}C-NMR (100 MHz, $CDCl_3$): δ 21.1, 43.6, 64.7, 111.6, 116.2, 119.8, 121.3, 124.3, 126.4, 126.6, 128.0, 128.7, 129.3, 129.8, 130.8, 131.4, 137.5, 138.5, 138.7, 144.3, 151.8, 152.7, 159.6, 164.1.

2.2.1.4 3-(2-(5-(4-Methoxyphenyl)-3-phenyl-4,5-dihydropyrazol-1-yl)thiazol-4-yl)-2H-chromen-2-one **(4)**.

Pale yellow solid; m.p. 242°C, Yield = 85%; **FT-IR** (ATR, cm^{-1}): ν_{max} 3153, 1712, 1604, 1552, 1512, 1330, 1242, 1118, 1027, 1004, 754; ^{1}H-NMR (400 MHz, $CDCl_3$): δ 3.42 (1H, dd, J_{cis} = 6.9Hz, J_{gem} = 18Hz, CH-pyrazoline), 3.72 (3H, s, OCH_3), 4.06 (1H, dd, J_{trans} = 12Hz, J_{gem} = 18Hz, CH-pyrazoline), 5.65 (1H, dd, J_{cis} = 6.9Hz, J_{trans} = 12Hz, CH-pyrazoline), 6.95-7.84 (14H, m, Ar), 8.32 (1H, s, CH-thiazole); ^{13}C-NMR (100 MHz, $CDCl_3$): δ 43.3, 55.5, 64.3, 111.5, 114.3, 116.3, 119.5, 120.9, 125.2, 126.9, 128.9, 129.1, 129.3, 130.5, 131.4, 132.1, 133.9, 138.8, 144.3, 152.7, 153.7, 159.0, 159.2, 164.0.

2.3 Crystal structure determination

Suitable crystals having proper size and shape of all synthesized compounds (**1**-**4**), were selected and analyzed by X-ray diffraction technique. Suitable crystal of each compound was coated with paratone oil and mounted on a glass fiber. All measurements were made on Bruker Kappa Apex-

IICCD diffractometer with graphite monochromator using M_o-K_α radiation source. All structures were solved by direct method and refined by using *SHELXL* 2013 (Sheldrick, 2013) [44]. The figures were plotted with *ORTEP* II program [45]. The CIF files of compounds (**1**-**4**) have been assigned CCDC numbers 1009293, 1009294, 981486, and 1009299 and can be obtained free of charge on application to CCDC 12 Union Road, Cambridge CB21 EZ, UK. (Fax: (+44) 1223 336-033: data_request@ccdc.cam.ac.uk).

2.4 Computational methods

DFT studies were performed with Gaussian 09 software [46]. Visualization of geometries and graphics were performed with GaussView 05 [47]. The geometries of all compounds (**1**-**4**) were optimized at hybrid B3LYP method along with 6-31G(d,p) basis set. B3LYP method is quite reliable for the structural properties of organic compounds, due to its nice balance between cost and accuracy [48–52]. These structures were confirmed as true minima through frequency analysis at the same level (no imaginary frequency). Furthermore, the results from frequency simulations were used for theoretical vibrational analysis. TD-DFT calculations for absorption spectra were performed at CAM-B3LYP/6-31G(d,p) level in DMSO solvent through CPCM model. Twenty excited states (10 each for singlet & triplet) were considered for the computation of absorption spectra of all compounds. Frontier molecular orbitals (FMOs) and molecular electrostatic potential (MEP) analyses were performed at B3LYP/6-31G(d,p) level of theory.

2.5 Determination of in-vitro AChE inhibitory activity

AChE (Electric eel type-VI-S, Sigma-Aldrich GmbH USA, code 1001596210), Acetylthiocholine iodide (Sigma-Aldrich UK, code 101303874), DTNB (Sigma Aldrich Germany, code 101261619), Galantamine hydrobromide Lycoris sp. (Sigma-Aldrich France, code G1660) and all the other chemicals used were of analytical grade. Galantamine was used as a reference drug.

The synthesized compounds (**1**-**4**) were dissolved in 0.1M phosphate buffer of pH 8.0 (KH_2PO_4/K_2HPO_4). The reaction mixture consisted of appropriate amount of DTNB (Ellman's reagent), test compounds and 0.03 U/mL of enzymes (AChE). The mixture was pre-incubated at 30 ^oC for 10 minutes and after that 1mM of ATCI was added and incubated again for further 15 minutes. The enzymatic hydrolysis was monitored at 412nm using lQuant microplate spectrophotometer (MQX200, BioTek USA). All reactions were repeated in triplicate. The IC_{50} values were determined by plotting the inhibition against the sample solution concentrations [53].

2.6 Molecular docking

Molecular docking studies were carried out using X-ray crystal structure of *Tc*AChE (PDB code 1EVE) co-crystalized with E2020. The structures of the compounds were drawn using MarvinSketch 16.5.2 [54]. Optimized structures of all compounds (**1-4**) from DFT studies were used for docking studies. For the enzyme, downloaded from PDB, solvation parameters and Kollman charges for all the atoms were assigned. AutoDock Tools (ADT) were used to create PDBQT file for both ligand and enzyme. A grid parameter file was generated using ADT. A cubic grid box of 40 Å (x, y, z) with a spacing of 0.375 Å was created. The grid map was created and centered in the active site region where E2020 (native ligand) was embedded (X=2.858421; Y=64.578837; Z=67.967228). As a first step, the reliability of docking algorithm was confirmed

by re-docking of co-crystalized ligand E2020 in the 1EVE pocket. The RMSD between the co-crystallized and re-docked conformation is 1.34 Å. The RMSD value of <2.0 Å is considered accurate in predicting binding orientation of ligand. To evaluate the lowest binding energy, docking studies were carried out using AutDock and a Lamarckian genetic algorithm (LGA) [55]. The maximum number of energy evaluations of the (LGA) run was 2500,000 and the maximum number of evaluations were set to 27,000. Other parameters were set to default values of AutoDock 4.2. The view of the docking results and analysis of their surface with graphical representations were done using AutoDock and discovery studio visualizer [56].

3. Results and discussion

The reaction sequence employed for the synthesis of target heterocycles is outlined in the Fig.1. Treatment of substituted chalcones, prepared by the reaction of acetophenone and substituted benzaldehydes under basic conditions, with thiosemicarbazide in the presence of NaOH afforded 3-Phenyl-5-substituted phenyl-4,5-dihydropyrazole-1-carbothioamide which on reaction with 3-(2-bromoacetyl)-2*H*-chromen-2-one furnished the target compounds (**1**-**4**). The analytical and spectral data of the molecules **1**-**4** was fully in agreement with the proposed structure. In the IR spectra, the appearance of absorption band for the carbonyl of lactone moiety in the range of 1718-1705 cm^{-1} and disappearance of doublet for NH_2 stretching in the range of 3500-3300 cm^{-1} confirmed the formation of derivatives (**1**-**4**) and agree well with the reported values in literature [57]. In ^{1}H NMR spectra, a singlet in the range δ 8.19–8.32 ppm assigned to CH proton of the thiazole, confirmed successful synthesis of desired compounds **1**-**4**. The protons in pyrazoline ring appeared as doublet of doublet in the range of 3.32-5.65 ppm also supported the synthesis [58,59]. In the ^{13}C NMR spectra, the low field resonance in the region of 164.1-164.0 and 159.8-159.2

were assigned to C=O of coumarin and C=N of thiazole moiety respectively. The other substituents and aromatic carbons were also fully analyzed (cf. Experimental section).

3.1 Molecular structure

The *ORTEP* plots of all compounds (**1**-**4**) are shown in Fig. 2, and structural refinement parameters are given in Table 1. The molecular formulas of the compounds (**1-4)** are $[C_{27}H_{18}BrN_3O_2S]$, $[C_{28}H_{21}N_3O_3S]$, $[C_{28}H_{21}N_3O_2S]$ and $[C_{28}H_{21}N_3O_3S]$, respectively. The compound (**1**) crystallized in orthorhombic crystal system having space group $Pca2_1$. Packing diagram (Fig. 3) shows that it consists of two independent molecules. In the first molecule, the chromen-2-one moiety A (C1-C9/O1/O2), 1,3-thiazol ring B (C10-C12/N1/S1), the pyrazol ring C (C13/C20/C21/N2/N3), the 3-bromophenyl D (C14-C19/BR1) and the benzene ring E (C22-C27) (atomic labelling is in accordance with the ORTEP plot Fig. 2) are planar with r. m. s. deviation of 0.0208, 0.0114, 0.0147, 0.0273 and 0.0041 Å, respectively. The dihedral angle between A/B, A/C, A/D, A/E, B/C, B/D, B/E, C/D, C/E and D/E are 12.6(4)°, 8.4(4)°, 75.4(2)°, 3.5(5)°, 8.5 (5)°, 87.4(3)°, 11.8(5)°, 79.8(3)°, 5.5(6)° and 75.6(3)°, respectively. In the second molecule, the chromen-2-one moiety F (C28-C36/O3/O4), 1,3-thiazol ring G (C37-C39/N4/S2), the pyrazol ring H (C40/C47/C48/N5/N6), the 3-bromophenyl I (C41-C46/BR2) and the benzene ring J (C49-C54) are planar with r. m. s. deviation of 0.0340, 0.0029, 0.0160, 0.0218 and 0.0069 Å, respectively. The dihedral angle between F/G, F/H, F/I, F/J, G/H, G/I, G/J, H/I, H/J and I/J are 9.1(4)°, 6.6(4)°, 83.6(2)°, 1.7(5)°, 10.0 (5)°, 83.3(3)°, 9.5(5)°, 84.3(3)°, 5.0(6)° and 83.2(3)°, respectively. The molecules exists in dimer form due to C-H…O interactions with $R_2^2(12)$ ring, where CH is of the thiazol ring and O-atoms are of the carbonyl groups. Those are further interlinked due to C-H…O bonding where H is from the dihydro carbon of the pyrazol ring and O-atom is of carbonyl group.

The presence of π-π interactions in the range 2.319(5)-3.582(2) Å and C-H…π interactions among different moieties collectively play important role in stabilizing the molecules.

The compound **2,** crystallized with monoclinic crystal system and $P2_1/c$ space group. The chromen-2-one moiety A (C1-C9/O1/O2), 1,3-thiazol ring B (C10-C12/N1/S1), the pyrazol ring C (C13/C21/C22/N2/N3), the 3-methoxyphenyl moiety D (C14-C20/O3) and the benzene ring E (C23-C28) in **2** are planar with r. m. s. deviation of 0.0403, 0.0027, 0.0343, 0.0218 and 0.0010 Å, respectively. The dihedral angle between rings A/B, A/C, A/D, A/E, B/C, B/D, B/E, C/D, C/E and D/E are 6.70(7)°, 1.58(9)°, 86.15(5)°, 1.42(8)°, 7.56(10)°, 88.80(7)°, 8.02(10)°, 84.60(7)°, 1.89(10)° and 85.57(7)°, respectively. The molecules are dimerized due to C-H…O interactions with $R_2^2(28)$ rings, where CH of the benzene ring in the chromen-2-one moiety and O-atom is of methoxy group. The π-π interactions are in the range 2.4842(10)-3.4805(10) Å. Moreover, some C-H…π interactions are also present and collectively with π-π interactions play important role in stabilizing the molecules.

The compound **3** has triclinic crystal system and *P*-1 space group. Again in **3**, the chromen-2-one moiety A(C1-C9/O1/O2), 1,3-thiazol ring B(C10-C12/N1/S1), the pyrazol ring C (C13/C21/C22/N2/N3), the 4-methylphenyl moiety D (C14-C20) and the benzene ring E (C23-C28) are planar with r. m. s. deviation of 0.0256, 0.0017, 0.0368, 0.0098 and 0.0021 Å, respectively. The dihedral angles between A/B, A/C, A/D, A/E, B/C, B/D, B/E, C/D, C/E and D/E are 9.30(8)°, 7.88(10)°, 76.69(5)°, 5.71(10)°, 6.76(12)°, 82.44(5)°, 15.00(11)°, 75.71(6)°, 12.28(12)° and 72.82(6)°, respectively. The individual molecules in **3**, are dimerized due to C-H…O interactions with $R_2^2(12)$ ring, where CH is of the thiazol ring and O-atom is of the carbonyl group. The dimmers are further interlinked due to C-H…O bonding where H is from the

dihydro carbon of pyrazol ring and O-atom is of the carbonyl group. There are π-π interactions are observed in the range of 2.5088(8)-4.40952(8) Å between the coumarin moieties.

Similarly in **4,** the chromen-2-one moiety A(C1-C9/O1/O2), 1,3-thiazol ring B(C10-C12/N1/S1), the pyrazol ring C(C13/C21/C22/N2/N3), the 4-methoxyphenyl moiety D (C14-C20/O3) and the benzene ring E (C23-C28) are planar with r. m. s. deviation of 0.0134, 0.0011, 0.0468, 0.0180 and 0.0036 Å, respectively. The dihedral angle between A/B, A/C, A/D, A/E, B/C, B/D, B/E, C/D, C/E and D/E are 2.47(8)°, 3.54(8)°, 86.73(7)°, 0.80(9)°, 4.47(9)°, 87.44(10)°, 2.45(10)°, 89.98(11)°, 4.33(10)° and 86.02(10)°, respectively. There π-π interactions in the range of 3.430(2)-4.146(2) Å. Moreover, some C-H…π interactions are present which collectively with π-π interaction play important role in stabilizing the molecules.

3.2 DFT Optimized geometries

The geometries of all four compounds have been optimized (Fig. 4) through DFT methods to compare the geometric parameters (bond lengths and bond angles) obtained theoretically with the X-ray diffraction results. The input geometries are taken from the X-ray structures. The important X-ray geometric parameters of all compounds (**1**-**4**) are given in Tables 2-3 (bond lengths) and Tables 4-5 (bond angles). The computed geometric parameters of bond lengths and bond angles are summarized in Table 3 and Table 5, respectively. The data given in the Tables, indicate that the X-ray geometric parameters have shown strong agreement with the theoretical results.

The X-ray values of important bond lengths involving hetro atoms such as Br1—C1, S1—C17, S1—C16, O1—C20, O2—C21, O2—C20, N1—C9, N1—N2, N2—C16, N2—C7, N3—C16, N3—C18 (atomic labelling is in accordance with Fig. 2) in **1** are 1.90, 1.72, 1.74, 1.20, 1.36, 1.38,

1.28, 1.38, 1.36, 1.48, 1.28 and 1.42Å, respectively. Whereas the corresponding theoretical values are 1.91, 1.74, 1.76, 1.21, 1.36, 1.38, 1.29, 1.37, 1.37, 1.48, 1.29 and 1.39Å respectively. In compound **2**, the important bonds such as S1—C11, S1—C12, O1—C9, O2—C1, O2—C9, O3—C18 O3—C20, N1—C12, N1—C10, N2—C12, N2—N3, N2—C13, N3—C22 determined experimentally are 1.71, 1.73, 1.20, 1.37, 1.37, 1.37, 1.40, 1.29, 1.38, 1.34, 1.37, 1.47 and 1.28Å, respectively. The simulated values of these bonds are 1.74, 1.76, 1.21, 1.39, 1.39, 1.36, 1.42, 1.29, 1.38, 1.37, 1.37, 1.48 and 1.29Å, respectively. Again, in compound **3** and **4** the basic skeleton is similar, only difference exists in the substituent on one aromatic ring. The experimental (X-ray) and simulated bond lengths of both compounds are in strong agreement with each other (for detailed values see Table 2 and Table 3).

The experimental and simulated values of all prominent bond angles of compounds (**1**-**4**) are narrated in Table 4 and 5, respectively. The comparative analysis shows that excellent correlation exists among experimental and theoretical values of bond angles of all compounds. In compound **1**, the experimental values of important bond angles such as C17—S1—C16, C21—O2—C20, C9—N1—N2, C16—N2—N1, C16—N2—C7, N1—N2—C7, C16—N3—C18, C6—C1—Br1, C2—C1—Br1, N1—C9—C8, N1—C9—C10, N3—C16—N2, N3—C16—S1, N2—C16—S1, C17—C18—N3, N3—C18—C19, O1—C20—O2, O1—C20—C19, O2—C20—C19, O2—C21—C27 and O2—C21—C22 are 88.0, 122.7, 106.8, 120.6, 123.3, 114.1, 110.1, 118.0, 120.5, 114.8, 122.1, 123.3, 116.1, 120.5, 113.8, 116.4, 116.3, 126.5, 117.2, 116.9 and 121.7^{o}, respectively. The theoretical values of these bond angles are 87.7, 123.5, 109.3, 119.1, 122.7, 113.5, 110.5, 119.1, 119.1, 112.8, 122.2, 123.1, 115.6, 121.1, 115.2, 117.3, 116.2, 126.7, 116.6, 117.6 and 120.7^{o}, respectively. Similarly, the experimental and theoretical bonds angles values in compounds **2**, **3** and **4** also corroborated nicely to each other.

3.3 Vibrational analysis

Since last few years, the DFT calculations have been extensively used to compare and validate the experimental vibrational spectrum [60–62]. The experimental FT-IR of all compounds were recorded under neat conditions and theoretical vibrational frequencies were extracted from the frequency analysis. The calculated vibrational spectrum of compound **2** is compared with the experimental spectrum in the Fig. 5. The calculated vibrational spectra of compounds **1**, **3** and **4** along with experimental spectra are given in Fig. S9 (supplementary information). The comparative analysis of prominent experimental and theoretical vibrations of all compounds is given in Table 6. In order to minimize the error, 0.9627 scaling factor was used, which is recommended for B3LYP/6-31G(d,p) level of theory [63,64]. The basic skeleton is same (compounds **1**-**4**), the only difference exists in the substituents on one aromatic ring. Therefore, the theoretical and experimental stretching/bending vibrations of prominent functional groups show similar kind of trends in vibrational spectra and correlate to each other nicely (experimentally as well as theoretically). The calculated prominent CH_{arom}. symmetric/asymmetric stretching vibrations of compounds **1**, **3** and **4** are 3089 cm^{-1} and 3080 cm^{-1}, of **2** are 3089 cm^{-1}, 3080 cm^{-1}, 2967 cm^{-1} and 2906 cm^{-1}. Their respective experimental values are 3123cm^{-1} (**1**), 3145 cm^{-1} (**2**), 3141 cm^{-1} (**3**) and 3153 cm^{-1} (**4**) respectively, which agree well with the computed values. Experimental value of stretching vibrations of C=O for compounds **1**, **2**, **3** and **4** are 1709 cm^{-1}, 1705 cm^{-1}, 1718 cm^{-1} and 1712 cm^{-1}, respectively. The theoretical stretching value for the carbonyl functional group is 1748 cm^{-1} in all four compounds. The experimental symmetric/asymmetric stretching vibrations of C=N functional group in all compounds (**1**-**4**) are

in the range 1545-1300 cm^{-1} and showed an excellent correlation with the theoretical values, (1550-1300 cm^{-1}). Apart from the stretching vibrations, number of bending vibrations of CH_3, CH_2 and aromatic CH groups are analyzed which also show nice correlation between theory and experiment (for individual values see Table 6). The experimental S-CH stretching vibrations are 752 cm^{-1}, 751 cm^{-1}, 752 cm^{-1} and 754 cm^{-1} for compound 1, 2, 3 and 4 respectively, whereas the theoretical bending vibrations appear at 751 cm^{-1} in all compounds (**1**-**4**).

3.4 Absorption studies and frontier molecular orbitals (FMOs) analysis

The experimental absorption maxima of all four compounds (**1**-**4**) were recorded in dimethyl sulfoxide (DMSO) solvent. The corresponding simulated absorption spectra were calculated by using time dependent (TD) calculation at CAM-B3LYP/6-31G(d,p) level of theory in DMSO by using conductor-like polarizable continuum model **(**CPCM). The experimental as well as theoretical absorption spectra of all compounds are shown in Fig. 6. In all compounds, almost similar chromophoric groups are present, therefore similar trends are observed in absorption maxima. The experimental absorption maxima are 352 nm (**1**), 354 nm (**2**), 352 nm (**3**) and 355 nm (**4**), respectively. Theoretically measured absorption maxima of all four derivatives (**1**-**4**) are 331 nm, 332 nm, 333 nm and 334 nm, respectively and correlated nicely with the experimental results. The differences are attributed to the errors associated with function in properly calculating the absorption spectrum.

Frontier molecular orbital (FMOs) analysis by using quantum chemical methods can be used to explain the molecular transitions and reactivity of compounds. The frontier molecular orbital analysis of all four compounds has been analyzed for correlation of theoretical and experimental

absorption spectra. In case of **1**, the corresponding HOMO and LUMO energies are -5.26 eV and -1.83 eV, respectively. The HOMO-LUMO gap is 3.43 eV, corresponds to 361 nm which is in excellent agreement the experimental transition at 352 nm. In compound **2**, the HOMO and LUMO energies are -5.12 eV and -1.73 eV, respectively. The HOMO-LUMO gap is 3.39 eV, which corresponds to transitions at 365 nm, which is again in complete agreement with experimental absorption maxima (354 nm). Similarly, in **3**, the corresponding HOMO (-5.13 eV) and LUMO (-1.76 eV) energies and HOMO-LUMO gap (3.37 eV) corroborated nicely with the experimental absorption maximum. The similar trend is observed for compound **4**. The HOMO-LUMO gap (3.34 eV) is in nice agreement with the experimental absorption band. The absorption maxima in all compounds reflect that molecular transitions are due to π to π^* (HOMO to LUMO) transitions of electrons. The HUMO and LUMO surfaces of all compounds are studied to understand the distribution of isodensities, and similar kind of trend is observed (For FMOs surfaces see the supplementary information Fig. S10).

3.5 Molecular electrostatic potential analysis

Molecular electrostatic potential analysis of all compounds was performed by using optimized geometries at B3LYP/6-31G(d,p) level of theory, and surfaces are shown in Fig. 7. From MEP surfaces it is observed that the –ve potential is concentrated on the coumarin moiety whereas the rest of the skeleton in all compounds is neutral. This reflects that all compounds are nucleophilic in nature. The dispersion of potential in ranges from -0.05796 to 0.05796 in **1**, -0.06007 to 0.06007 in **2**, -0.05939 to 0.05939 in **3** and -0.0591 to 0.0591 esu in **4**, respectively. The maximum dispersion is observed in **2**, which reflects that **2** has more affinity for electropositive charge.

3.6 Acetyl Cholinesterase (AChE) inhibition potential

To find out the therapeutic potential of the thiazoles derivatives bearing coumarin moiety in the treatment of AD, the inhibitory response of compounds **1–4** together with the reference standard galantamine against AChE was evaluated as per Ellman's protocol by determining the rate of acetylthiocholine in the presence of the inhibitor. All compounds proved to be immensely active toward AChE in low micromolar range of IC_{50} values. The in-vitro AChE inhibitory response (IC_{50} values) of the target compounds are summarized in Table 7. From the data, it is notable that among the four compounds tested, compound **3** exhibited the highest inhibitory activity toward AChE, which is even higher than galantamine (44.02 µM), a standard drug. Compound **3**, emerged as potent compound with IC_{50} value of 27.29 ± 0.42 µM, followed by compound **1** with IC_{50} value of 70.94 ± 0.29 µM. The compounds **2** and **4** showed poor inhibition with IC50 values of 3461.43 µM and 1113 µM respectively.

3.7 Molecular docking studies

To evaluate the binding affinity of the experimentally tested compounds, docking studies were carried out using AutoDock 4.2 [65]. Molecular docking studies were carried out using X-ray crystal structure of *Tc*AChE (PDB code 1EVE) [66]. Three dimensional (3D) modelled molecular surface of compound **3** (IC_{50}=27.29 µM) into the binding site of 1EVE is shown in Fig. 8. The visual inspection of the lowest energy docked pose of compound **3** showed that the coumarin ring is oriented toward the catalytic anionic site (CAS) and forms strong bifurcated π-π stacking

interactions with indole ring of Trp84. 3-Methoxyphenyl ring establishes π-π stacking interactions with peripheral anionic site (PAS) residues Trp279 at the entry of the active site gorge. Another important PAS residue Tyr121 forms four types of interactions with compound **3**. Two hydrogen bonding interactions were also observed between the carbonyl oxygen of coumarin and OH of Tyr121. The phenyl ring of Tyr121 also forms one π-π T-shaped interactions with the thiazole ring and one π-sulphur interaction with its sulphur atom. A π-non-bonding electron interaction was also observed between OH of Tyr121 and thiazole ring π-system. Tyr70 is another PAS residue, which forms π-sulphur interaction with its sulphur atom of the thiazole (Fig. 9). The free energy of binding for compound **3** is -11.92 kcal mol^{-1}.

4. Conclusions

Four new *3-(2-(3-Phenyl-5-substituted phenyl-4,5-dihydropyrazol-1-yl)thiazol-4-yl)-2H-chromen-2-one* **1-4** containing coumarin, 2-pyrazoline clubbed with 1,3-thiazole scaffold were synthesized in very good yield. Characterization of final structures was achieved with help of spectroscopic and X-ray diffraction analyses. Calculated bond lengths and bond angles of all compounds correlated very nicely with the X-ray values. The experimental and theoretical vibrations of all prominent functional groups in all compounds are in good agreement with each other. The FMOs analysis proved that electronic transitions are mainly due to π to π* transitions. The low band gap reflects that compounds are reactive and kinetically less stable. The ESP analysis reveals that all four compounds (**1**-**4**) are nucleophilic in nature. The maximum dispersion of potential is observed in 2 (-0.06007 to 0.06007 esu). Compound **3** exhibited inhibitory activity toward AChE almost equal galantamine, a standard drug and emerged as potent compound with IC_{50} value of 27.29 ±

0.42 μM. Molecular docking studies proved that the free energy of binding is maximum compound **3** (-11.92 kcal mol^{-1}).

Acknowledgements

The authors highly acknowledge Higher Education Commission of Pakistan (Grant no. 20-3013/NRPU/R&D/HEC/14/525), QAU Islamabad, COMSATS Abbottabad and University of Azad Jammu and Kashmir for financial support.

Supplementary material

Cartesian co-ordinates of optimized geometries and cif files of all four compounds (**1**-**4**) are provided in supporting information. Experimental ^{1}H, ^{13}C-NMRs are also pasted in supporting information as Fig. S1-S8. The combined experimental and theoretical IRs of compounds **1**, **3** and **4** are provided in Fig. S9 and HOMO-LUMO surfaces are given in the Fig. S10. Supplementary data associated with this article can be found, in the online version, at http://dx.doi.org/

References

[1] R. Aggarwal, S. Kumar, P. Kaushik, D. Kaushik, G.K. Gupta, Synthesis and pharmacological evaluation of some novel 2-(5-hydroxy-5-trifluoromethyl-4,5-dihydropyrazol-1-yl)-4-(coumarin-3-yl)thiazoles, Eur. J. Med. Chem. 62 (2013) 508–514.

[2] L. Yurttaş, Y. Özkay, H. Karaca Gençer, U. Acar, Synthesis of Some New Thiazole Derivatives and Their Biological Activity Evaluation, J. Chem. 2015 (2015) 1–7.

[3] A. Leoni, A. Locatelli, R. Morigi, M. Rambaldi, Novel thiazole derivatives: a patent review (2008 – 2012; Part 1), Expert Opin. Ther. Pat. 24 (2014) 201–216.

[4] D.S.N. Bikobo, D.C. Vodnar, A. Stana, B. Tiperciuc, C. Nastasă, M. Douchet, O. Oniga, Synthesis of 2-phenylamino-thiazole derivatives as antimicrobial agents, J. Saudi Chem. Soc. 21 (2017) 861–868.

[5] O.I. El-Sabbagh, M.M. Baraka, S.M. Ibrahim, C. Pannecouque, G. Andrei, R. Snoeck, J. Balzarini, A.A. Rashad, Synthesis and antiviral activity of new pyrazole and thiazole derivatives, Eur. J. Med. Chem. 44 (2009) 3746–3753.

[6] M.M. Mohy El-Din, A.M. Senbel, A.A. Bistawroos, A. El-Mallah, N.A. Nour El-Din, A.A. Bekhit, H.A. Abd El Razik, A Novel COX-2 Inhibitor Pyrazole Derivative Proven Effective as an Anti-Inflammatory and Analgesic Drug, Basic Clin. Pharmacol. Toxicol. 108 (2011) 263–273.

[7] V. Zaharia, A. Ignat, N. Palibroda, B. Ngameni, V. Kuete, C.N. Fokunang, M.L. Moungang, B.T. Ngadjui, Synthesis of some p-toluenesulfonyl-hydrazinothiazoles and hydrazino-bis-thiazoles and their anticancer activity, Eur. J. Med. Chem. 45 (2010) 5080–5085.

[8] K.W. Woods, R.W. McCroskey, M.R. Michaelides, C.K. Wada, K.I. Hulkower, R.L. Bell, Thiazole analogues of the NSAID indomethacin as selective COX-2 Inhibitors, Bioorg. Med. Chem. Lett. 11 (2001) 1325–1328.

[9] F. Jorquera, M.M. Almar, A. Jimeno, M. González-Sastre, J. González-Gallego, Assessment of antipyrine kinetics from saliva or plasma: influence of age, J. Pharm.

Biomed. Anal. 13 (1995) 1141–1145.

[10] A.K. Tewari, P. Srivastava, V.P. Singh, A. Singh, R.K. Goel, C.G. Mohan, Novel Anti-inflammatory Agents Based on Pyrazole Based Dimeric Compounds; Design, Synthesis, Docking and in Vivo Activity, Chem. Pharm. Bull. (Tokyo). 58 (2010) 634–638.

[11] A. Kamal, K.S. Reddy, M.N.A. Khan, R.V.C.R.N.C. Shetti, M.J. Ramaiah, S.N.C.V.L. Pushpavalli, C. Srinivas, M. Pal-Bhadra, M. Chourasia, G.N. Sastry, A. Juvekar, S. Zingde, M. Barkume, Synthesis, DNA-binding ability and anticancer activity of benzothiazole/benzoxazole–pyrrolo[2,1-c][1,4]benzodiazepine conjugates, Bioorg. Med. Chem. 18 (2010) 4747–4761.

[12] F. Azam, B.A. El-gnidi, I.A. Alkskas, M.A. Ahmed, Design, synthesis and anti-Parkinsonian evaluation of 3-alkyl/aryl-8-(furan-2-yl)thiazolo[5,4- e][1,2,4]triazolo[1,5- c]pyrimidine-2(3 H)-thiones against neuroleptic-induced catalepsy and oxidative stress in mice, J. Enzyme Inhib. Med. Chem. 25 (2010) 818–826.

[13] R.N. Sharma, F.P. Xavier, K.K. Vasu, S.C. Chaturvedi, S.S. Pancholi, Synthesis of 4-benzyl-1,3-thiazole derivatives as potential anti-inflammatory agents: An analogue-based drug design approach, J. Enzyme Inhib. Med. Chem. 24 (2009) 890–897.

[14] I. Kostova, S. Raleva, P. Genova, R. Argirova, Structure-Activity Relationships of Synthetic Coumarins as HIV-1 Inhibitors, Bioinorg. Chem. Appl. 2006 (2006) 1–9.

[15] S. Ben Mohamed, Y. Rachedi, M. Hamdi, F. Le Bideau, C. Dejean, F. Dumas, An Efficient Synthetic Access to Substituted Thiazolyl-pyrazolyl-chromene-2-ones from Dehydroacetic Acid and Coumarin Derivatives by a Multicomponent Approach, European J. Org. Chem.

2016 (2016) 2628–2636.

[16] K. Vaarla, R.K. Kesharwani, K. Santosh, R.R. Vedula, S. Kotamraju, M.K. Toopurani, Synthesis, biological activity evaluation and molecular docking studies of novel coumarin substituted thiazolyl-3-aryl-pyrazole-4-carbaldehydes, Bioorg. Med. Chem. Lett. 25 (2015) 5797–5803.

[17] X. Yu, D. Scheller, O. Rademacher, T. Wolff, Selectivity in the Photodimerization of 6-Alkylcoumarins, J. Org. Chem. 68 (2003) 7386–7399.

[18] A. Al-Kawkabani, M. Makhloufi-Chebli, N. Benosmane, B. Boutemeur-Kheddis, M. Hamdi, A.M.S. Silva, Study of the novel fluorescent 4-methyl-9-(3-oxobutanoyl)-2 H ,8 H -pyrano[2,3- f]chromene-2,8-dione derivative. Estimation of the ground- and excited-state dipole moments from a solvatochromic shift, J. Mol. Struct. 1146 (2017) 285–291.

[19] H.N. Harishkumar, K.M. Mahadevan, J.N. Masagalli, Facile Synthesis of 2-(1,3-Benzoxazol/benzothiazol-2-yl)- 3H-benzo[f]chromen-3-one as Blue Fluorescent Brighteners, S. Afr. J. Chem. 65 (2012) 5–9.

[20] S.H. Mashraqui, H. Mistry, S. Sundaram, π-Aryl/heteroaryl conjugated coumarin-thiazoles: Synthesis, optical spectral and nonlinear optic properties, J. Heterocycl. Chem. 43 (2006) 917–923.

[21] X. LI, Y. ZHAO, T. WANG, M. SHI, F. WU, Coumarin derivatives with enhanced two-photon absorption cross-sections, Dye. Pigment. 74 (2007) 108–112.

[22] K.-L. An, K.H. Park, K. Jun, A New Coumarin-Based Colorimetric and Fluorometric

Sensor for Cu 2+, Bull. Korean Chem. Soc. 35 (2014) 2183–2185.

[23] H.G. Bonacorso, M.B. Rodrigues, W.C. Rosa, L.B. Silva, C.P. Frizzo, N. Zanatta, M.A.P. Martins, Cyanoacetylazoles and salicylic aldehydes promoting the synthesis of new trifluoromethyl-substituted azolecarbonyl-2H-chromen-2-ones through the Knoevenagel condensation reaction, J. Fluor. Chem. 178 (2015) 296–305.

[24] D.P. Specht, P.A. Martic, S. Farid, Ketocoumarins, Tetrahedron. 38 (1982) 1203–1211.

[25] A.M. Palmer, Neuroprotective therapeutics for Alzheimer's disease: progress and prospects, Trends Pharmacol. Sci. 32 (2011) 141–147.

[26] A. V. Terry, The Cholinergic Hypothesis of Age and Alzheimer's Disease-Related Cognitive Deficits: Recent Challenges and Their Implications for Novel Drug Development, J. Pharmacol. Exp. Ther. 306 (2003) 821–827.

[27] R.E. Hughes, K. Nikolic, R.R. Ramsay, One for All? Hitting Multiple Alzheimer's Disease Targets with One Drug, Front. Neurosci. 10 (2016).

[28] I. Orhan, M. Aslan, Appraisal of scopolamine-induced antiamnesic effect in mice and in vitro antiacetylcholinesterase and antioxidant activities of some traditionally used Lamiaceae plants, J. Ethnopharmacol. 122 (2009) 327–332.

[29] E.J. Mufson, S.E. Counts, S.E. Perez, S.D. Ginsberg, Cholinergic system during the progression of Alzheimer's disease: therapeutic implications, Expert Rev. Neurother. 8 (2008) 1703–1718.

[30] I. Orhan, M. Abu-Asaker, F. Senol, T. Atici, B. Sener, M. Kartal, Antioxidant and

Anticholinesterase Assets and Liquid Chromatography-Mass Spectrometry Preface of Various Fresh-Water and Marine Macroalgae, Pharmacogn. Mag. 5 (2009) 291.

[31] I.A. Moussa, S.D. Banister, C. Beinat, N. Giboureau, A.J. Reynolds, M. Kassiou, Design, Synthesis, and Structure−Affinity Relationships of Regioisomeric N -Benzyl Alkyl Ether Piperazine Derivatives as σ-1 Receptor Ligands, J. Med. Chem. 53 (2010) 6228–6239.

[32] F. Caillé, F. Cacheux, M.-A. Peyronneau, B. Jego, E. Jaumain, G. Pottier, C. Ullmer, U. Grether, A. Winkeler, F. Dollé, A. Damont, B. Kuhnast, From Structure–Activity Relationships on Thiazole Derivatives to the In Vivo Evaluation of a New Radiotracer for Cannabinoid Subtype 2 PET Imaging, Mol. Pharm. 14 (2017) 4064–4078.

[33] A. Arshad, H. Osman, M.C. Bagley, C.K. Lam, S. Mohamad, A.S.M. Zahariluddin, Synthesis and antimicrobial properties of some new thiazolyl coumarin derivatives, Eur. J. Med. Chem. 46 (2011) 3788–3794.

[34] A.M. Vijesh, A.M. Isloor, V. Prabhu, S. Ahmad, S. Malladi, Synthesis, characterization and anti-microbial studies of some novel 2,4-disubstituted thiazoles, Eur. J. Med. Chem. 45 (2010) 5460–5464.

[35] U. Rashid, F. Rahim, M. Taha, M. Arshad, H. Ullah, T. Mahmood, M. Ali, Synthesis of 2-acylated and sulfonated 4-hydroxycoumarins: In vitro urease inhibition and molecular docking studies, Bioorg. Chem. 66 (2016) 111–116.

[36] M. Madni, S. Hameed, M.N. Ahmed, M.N. Tahir, N.A. Al-Masoudi, C. Pannecouque, Synthesis, crystal structure, anti-HIV, and antiproliferative activity of new pyrazolylthiazole derivatives, Med. Chem. Res. 26 (2017) 2653–2665.

[37] M. Madni, S. Hameed, M.N Ahmed, K.A. Yasin, M.N Tahir, Synthesis, Crystal Structure and DNA Interaction Study of 3-(2-(3, 5-Diphenyl-4, 5-dihydropyrazol-1-yl) thiazol-4-yl)-2H-chromen-2-one, Chinese J. Struct. Chem. 7 (2015) 1013-1018.

[38] M.N. Ahmed, B. Sadiq, N.A. Al-Masoudi, K.A. Yasin, S. Hameed, T. Mahmood, K. Ayub, M.N. Tahir, Synthesis, crystal structures, computational studies and antimicrobial activity of new designed bis((5-aryl-1,3,4-oxadiazol-2-yl)thio)alkanes, J. Mol. Struct. 1155 (2018) 403–413.

[39] S. Abbas, H.H. Nasir, S. Zaib, S. Ali, T. Mahmood, K. Ayub, M.N. Tahir, J. Iqbal, Carbonic anhydrase inhibition of Schiff base derivative of imino-methyl-naphthalen-2-ol: Synthesis, structure elucidation, molecular docking, dynamic simulation and density functional theory calculations, J. Mol. Struct. 1156 (2018) 193–200.

[40] M.N. Ahmed, K.A. Yasin, R.A.H. Khan, T. Mahmood, K. Ayub, D. Malik, M. Hafeez, A. M. Khan, M.N. Tahir, Synthesis, Crystal Structure, Spectral Analysis, DFT Studies and Antimicrobial Activity of Ethyl 6-(4-(ethoxycarbonyl)-1H-1,2,3-triazol-1-yl)pyridine-3-carboxylate, J. Chem. Soc. Pak. 39 (2017) 640-649.

[41] M.N. Arshad, N. Kosar, A.M. Asiri, K. Ayub, I.U. Khan, T. Mahmood, Synthesis and Structural Properties of N-(2-bromo-4-nitrophenyl)-3-methoxy-4-oxo-3,4-dihydro-2H-benzo[e][1,2]thiazine-3-carboxamide 1,1-dioxide: A Comparative Experimental and Quantum Chemical Study, J. Chem. Soc. Pak., 39 (2017) 727-736.

[42] Y.-M. Lin, Y. Zhou, M.T. Flavin, L.-M. Zhou, W. Nie, F.-C. Chen, Chalcones and flavonoids as anti-Tuberculosis agents, Bioorg. Med. Chem. 10 (2002) 2795–2802.

[43] B.F. Abdel-Wahab, H.A. Abdel-Aziz, E.M. Ahmed, Synthesis and antimicrobial evaluation of 1-(benzofuran-2-yl)-4-nitro-3-arylbutan-1-ones and 3-(benzofuran-2-yl)-4,5-dihydro-5-aryl-1-[4-(aryl)-1,3-thiazol-2-yl]-1H-pyrazoles, Eur. J. Med. Chem. 44 (2009) 2632–2635.

[44] G.M. Sheldrick, A short history of SHELX, Acta Crystallogr. Sect. A Found. Crystallogr. 64 (2008) 112–122.

[45] L.J. Farrugia, WinGX and ORTEP for Windows : an update, J. Appl. Crystallogr. 45 (2012) 849–854.

[46] J.L. W.C. Frisch, M.J.; Trucks, G.W.; Schlegel, H.B.; Scuseria, G.E.; Robb, M.A.; Cheeseman, J.R.; Scalmani, G.; Barone, V.; Mennucci, B.; Petersson, G.A.; Nakatsuji, H.; Caricato, M.; Li, X.; Hratchian, H.P.; Izmaylov, A.F.; Bloino, J.; Zheng, G.; Sonnenberg, Gaussian 09, Rev. C.01, Gaussian, Inc., Wallingford CT, 2010.

[47] R. Dennington, T. Keith, J. Millam, GaussView 05, Semichem Inc., 2009.

[48] R.U. Nisa, M.A. Hashmi, S. Sajjad, T. Mahmood, J. Iqbal, K. Ayub, Quantum mechanical investigation on acceleration of electrocyclic reactions through transition metal catalysis, J. Organomet. Chem. 808 (2016) 78–86.

[49] A. Babar, H. Khalid, K. Ayub, S. Saleem, A. Waseem, T. Mahmood, M.A. Munawar, G. Abbas, A.F. Khan, Synthesis, characterization and density functional theory study of some new 2-anilinothiazoles, J. Mol. Struct. 1072 (2014) 221–227.

[50] M.N. Arshad, A.M. Asiri, K.A. Alamry, T. Mahmood, M.A. Gilani, K. Ayub, A.S. Birinji, Synthesis, crystal structure, spectroscopic and density functional theory (DFT) study of N-

[3-anthracen-9-yl-1-(4-bromo-phenyl)-allylidene]-N-benzenesulfonohydrazine, Spectrochim. Acta Part A Mol. Biomol. Spectrosc. 142 (2015) 364–374.

[51] R.U. Nisa, M. Maria, F. Wasim, T. Mahmood, R. Ludwig, K. Ayub, Mechanistic insight of TiCl 4 catalyzed formal [3 + 3] cyclization of 1,3-bis(silyl enol ethers) with 1,3-dielectrophiles, RSC Adv. 5 (2015) 94304–94314.

[52] Maria, M. Hanif, T. Mahmood, R. Ludwig, K. Ayub, Aromaticity of azines through dyotropic double hydrogen transfer reaction, J. Mol. Model. 20 (2014) 2304.

[53] M. Sarfraz, N. Sultana, U. Rashid, M.S. Akram, A. Sadiq, M.I. Tariq, Synthesis, biological evaluation and docking studies of 2,3-dihydroquinazolin-4(1 H)-one derivatives as inhibitors of cholinesterases, Bioorg. Chem. 70 (2017) 237–244.

[54] MarvinSketch, version 16.5.2, calculation module developed by ChemAxon, http://www.chemaxon.com/products/marvin/marvinsketch/, 2016.

[55] G.M. Morris, D.S. Goodsell, R.S. Halliday, R. Huey, W.E. Hart, R.K. Belew, A.J. Olson, Automated docking using a Lamarckian genetic algorithm and an empirical binding free energy function, J. Comput. Chem. 19 (1998) 1639–1662.

[56] Dassault Systèmes BIOVIA, Discovery Studio Modeling Environment, Release 4.5, San Diego: Dassault Systèmes, 2015.

[57] S. Pavurala, R.R. Vedula, Synthesis of 3-(2-(4,5-Dihydro-3,5-diphenylpyrazol-1-yl)thiazol-4-yl)-2 H -chromen-2-one Derivatives via Multicomponent Approach, Synth. Commun. 44 (2014) 583–588.

[58] C.S.R. Venkata, V.R. Rao, A Facile One-Pot Expeditious Synthesis of Thiazolyl-pyrazolones, Phosphorus. Sulfur. Silicon Relat. Elem. 186 (2011) 489–495.

[59] K. Srimanth, V. Rao, D. Krishna, Synthesis and Evaluation of Anticancer Activity of Some Imidazothiazolyl, Imidazobenzothiazolyl and Dihydroimidazothiazolyl Coumarins, Arzneimittelforschung. 52 (2011) 388–392.

[60] M.N. Ahmed, K.A. Yasin, K. Ayub, T. Mahmood, M.N. Tahir, B.A. Khan, M. Hafeez, M. Ahmed, I. Ul-Haq, Click one pot synthesis, spectral analyses, crystal structures, DFT studies and brine shrimp cytotoxicity assay of two newly synthesized 1,4,5-trisubstituted 1,2,3-triazoles, J. Mol. Struct. 1106 (2016) 430–439.

[61] T.U. Rahman, M. Arfan, T. Mahmood, W. Liaqat, M.A. Gilani, G. Uddin, R. Ludwig, K. Zaman, M.I. Choudhary, K.F. Khattak, K. Ayub, Isolation, spectroscopic and density functional theory studies of 7-(4-methoxyphenyl)-9H-furo[2,3-f]chromen-9-one: A new flavonoid from the bark of Millettia ovalifolia, Spectrochim. Acta Part A Mol. Biomol. Spectrosc. 146 (2015) 24–32.

[62] M.N. Ahmed, K.A. Yasin, S. Hameed, K. Ayub, I. Haq, M.N. Tahir, T. Mahmood, Synthesis, structural studies and biological activities of three new 2-(pentadecylthio)-5-aryl-1,3,4-oxadiazoles, J. Mol. Struct. 1129 (2017) 50–59.

[63] M. Arshad, M. Jadoon, Z. Iqbal, M. Fatima, M. Ali, K. Ayub, A.M. Qureshi, M. Ashraf, M.N. Arshad, A.M. Asiri, A. Waseem, T. Mahmood, Synthesis, molecular structure, quantum mechanical studies and urease inhibition assay of two new isatin derived sulfonylhydrazides, J. Mol. Struct. 1133 (2017) 80–89.

[64] S. Sherzaman, Sadiq-ur-Rehman, M.N. Ahmed, B.A. Khan, T. Mahmood, K. Ayub, M.N. Tahir, Thiobiuret based Ni(II) and Co(III) complexes: Synthesis, molecular structures and DFT studies, J. Mol. Struct. 1148 (2017) 388–396.

[65] G.M. Morris, R. Huey, W. Lindstrom, M.F. Sanner, R.K. Belew, D.S. Goodsell, A.J. Olson, AutoDock4 and AutoDockTools4: Automated docking with selective receptor flexibility, J. Comput. Chem. 30 (2009) 2785–2791.

[66] G. Kryger, I. Silman, J.L. Sussman, Structure of acetylcholinesterase complexed with E2020 (Aricept®): implications for the design of new anti-Alzheimer drugs, Structure. 7 (1999) 297–307.

Captions

Table 1: X-ray and structural parameters of all four compounds (**1-4**).

Table 2 Important X-ray bond lengths (Å) of compounds **1-4**, respectively (Atomic labels are with reference *ORTEP* plots Fig. 2).

Table 3: Simulated bond lengths (Å) of compounds **1-4**, respectively (Atomic labels are with reference *ORTEP* plots Fig. 2).

Table 4: Important X-ray bond angles (^{o}) of compounds **1-4**, respectively (Atomic labels are with reference *ORTEP* plots Fig. 2).

Table 5: Important X-ray bond angles (^{o}) of compounds **1-4**, respectively (Atomic labels are with reference *ORTEP* plots Fig. 2).

Table 6: Important experimental and simulated vibrations (cm^{-1}) of compounds **1-4**.

Table 7: AChE inhibition potential of all compounds (**1**-**4**).

Fig. 1: Synthetic scheme for the synthesis of coumarin based pyrazolylthiazole compounds (**1**-**4**).

Fig. 2: *ORTEP* plots of compounds **1**-**4**.

Fig. 3: Packing diagrams of compounds (**1**-**4**), showing the intermolecular hydrogen bonding.

Fig. 4: The optimized geometries of all compounds **1**-**4**.

Fig. 5: Combined experimental and simulated vibrational spectra of compound **2**.

Fig. 6: Combined Experimental and theoretical absorption spectra of all compounds (**1**-**4**).

Fig. 7: ESP surfaces of all compounds **1**-**4**.

Fig. 8: a) AutoDock generated pose of most active compound **3** into the binding site of AChE (PDB ID 1EVE); (b) Close-up depiction of the docking pose of compound **3** showing different types of ligand-enzyme interactions in the binding site of 1EVE. The key residues are represented as green stick mode.

Fig. 9: Close-up depiction of the docking pose of (a) compound **1**; (b) Compound **2** showing different types of ligand-enzyme interactions in the binding site of 1EVE.

Table 1: X-ray and structural parameters of all four compounds (**1-4**).

Compound No	**A-11**	**A-12**	**A-16**	**A-17**
CCDC No	**1009293**	**1009294**	**981486**	**1009299**
Chemical formula	$C_{27}H_{18}BrN_3O_2S$	$C_{28}H_{21}N_3O_3S$	$C_{28}H_{21}N_3O_2S$	$C_{28}H_{21}N_3O_3S$
M_r	528.41	479.54	463.54	479.54
Crystal system, space group	Orthorhombic, $Pca2_1$	Monoclinic, $P2_1/c$	Triclinic, P-1	Monoclinic, $C2/c$
Temperature (K)	293	296	296	296
a, b, c (Å)	19.4414 (19), 9.9342 (9), 23.8023 (18)	9.8734 (6), 20.6781 (12), 12.0370 (6)	10.2603 (7), 10.6009 (6), 11.1147 (8)	27.808 (6), 9.7320 (16), 21.708 (7)
α, β, γ (°)	----------	108.562 (2)	99.563 (2), 98.318 (3), 96.514 (2)	127.657 (4)
V (Å^3)	4597.1 (7)	2329.7 (2)	1167.82 (13)	4651 (2)
Z	8	4	2	8
Radiation type	Mo $K\alpha$	Mo $K\alpha$	Mo $K\alpha$	Mo $K\alpha$
μ (mm^{-1})	1.91	0.18	0.17	0.18
Crystal size (mm)	××	0.40 × 0.30 × 0.14	××	0.36 × 0.22 × 0.18
Diffractometer	?	?	?	?
Absorption correction	–	–	–	–
No. of measured, independent and observed [$I > 2\sigma(I)$] reflections	19152, 7734, 4395	19142, 5270, 3634	18053, 5053, 3530	18801, 5114, 1876
R_{int}	0.054	0.027	0.026	0.076
$(\sin \Theta/\lambda)_{max}$ (Å^{-1})	0.617	0.648	0.639	0.641
$R[F^2 > 2\sigma(F^2)]$, $wR(F^2)$, S	0.063, 0.176, 1.03	0.045, 0.121, 1.03	0.042, 0.125, 1.03	0.055, 0.140, 0.92
No. of reflections	7734	5270	5053	5114
No. of parameters	613	317	308	317
No. of restraints	1	H-atom	H-atom	H-atom

		parameters constrained	parameters constrained	parameters constrained
H-atom treatment	H-atom parameters constrained	0.25, -0.25	0.18, -0.22	0.15, -0.21

Table 2: Important X-ray bond lengths (Å) of compounds **1-4**, respectively (Atomic labels are with reference *ORTEP* plots Fig. 2).

1	Bond length	**2**	Bond length	**3**	Bond length	**4**	Bond length
Br1—C1	1.90 (13)	S1—C11	1.71 (19)	S1—C11	1.71 (18)	S1—C11	1.70 (3)
S1—C17	1.72 (10)	S1—C12	1.73 (18)	S1—C12	1.73 (17)	S1—C12	1.73 (3)
S1—C16	1.74 (11)	O1—C9	1.20 (2)	O1—C9	1.37 (2)	O1—C9	1.37 (3)
O1—C20	1.20 (12)	O2—C1	1.37 (2)	O1—C1	1.37 (2)	O1—C1	1.38 (3)
O2—C21	1.36 (12)	O2—C9	1.37 (2)	O2—C9	1.19 (19)	O2—C9	1.20 (3)
O2—C20	1.38 (12)	O3—C18	1.37 (3)	N1—C12	1.29 (2)	O3—C25	1.36 (4)
N1—C9	1.28 (12)	O3—C20	1.40 (3)	N1—C10	1.39 (19)	O3—C28	1.43 (3)
N1—N2	1.38 (10)	N1—C12	1.29 (2)	N2—C12	1.35 (2)	N1—C12	1.29 (3)
N2—C16	1.36 (12)	N1—C10	1.38 (2)	N2—N3	1.38 (19)	N1—C10	1.39 (3)
N2—C7	1.48 (12	N2—C12	1.34 (2)	N2—C15	1.46 (2)	N2—C12	1.36 (3)
N3—C16	1.28 (12)	N2—N3	1.37 (19)	N3—C13	1.28 (2)	N2—N3	1.38 (3)
N3—C18	1.42 (11)	N2—C13	1.47 (2)			N2—C13	1.47 (3)
		N3—C22	1.28 (2)			N3—C15	1.28 (3)

Table 3: Simulated bond lengths (Å) of compounds **1-4**, respectively (Atomic labels are with reference *ORTEP* plots Fig. 2).

1	Bond length	**2**	Bond length	**3**	Bond length	**4**	Bond length
Br1—C1	1.91	S1—C11	1.74	S1—C11	1.74	S1—C11	1.74
S1—C17	1.74	S1—C12	1.76	S1—C12	1.76	S1—C12	1.76
S1—C16	1.76	O1—C9	1.21	O1—C9	1.39	O1—C9	1.39
O1—C20	1.21	O2—C1	1.39	O1—C1	1.36	O1—C1	1.36
O2—C21	1.36	O2—C9	1.39	O2—C9	1.21	O2—C9	1.21
O2—C20	1.38	O3—C18	1.36	N1—C12	1.30	O3—C25	1.36
N1—C9	1.29	O3—C20	1.42	N1—C10	1.39	O3—C28	1.41
N1—N2	1.37	N1—C12	1.29	N2—C12	1.36	N1—C12	1.30
N2—C16	1.37	N1—C10	1.38	N2—N3	1.37	N1—C10	1.39
N2—C7	1.48	N2—C12	1.37	N2—C15	1.48	N2—C12	1.36
N3—C16	1.29	N2—N3	1.37	N3—C13	1.29	N2—N3	1.37
N3—C18	1.39	N2—C13	1.48			N2—C13	1.48
		N3—C22	1.29			N3—C15	1.29

Table 4: Important X-ray bond angles (°) of compounds **1**-**4**, respectively (Atomic labels are with reference *ORTEP* plots Fig. 2).

1	Bond angle	**2**	Bond angle	**3**	Bond angle	**4**	Bond angle
C17—S1—C16	88.0 (5)	C11—S1—C12	88.1 (8)	C11—S1—C12	87.7 (8)	C11—S1—C12	87.6 (14)
C21—O2—C20	122.7 (8)	C1—O2—C9	122.7 (13)	C9—O1—C1	122.8 (13)	C9—O1—C1	122.7 (2)
C9—N1—N2	106.8 (7)	C18—O3—C20	119.5 (3)	C12—N1—C10	109.4 (13)	C25—O3—C28	116.6 (3)
C16—N2—N1	120.6 (7)	C12—N1—C10	109.8 (14)	C12—N2—N3	119.6 (14)	C12—N1—C10	108.6 (2)
C16—N2—C7	123.3 (8)	C12—N2—N3	120.6 (15)	C12—N2—C15	126.0 (14)	C12—N2—N3	119.0 (2)
N1—N2—C7	114.1 (7)	C12—N2—C13	125.1 (14)	N3—N2—C15	114.2 (13)	C12—N2—C13	126.8 (2)
C16—N3—C18	110.1 (8)	N3—N2—C13	114.0 (14)	C13—N3—N2	107.7 (14)	N3—N2—C13	114.1 (2)
C6—C1—Br1	118.0 (10)	C22—N3—N2	108.0 (14)	O1—C1—C2	117.4 (16)	C15—N3—N2	108.1 (2)
C2—C1—Br1	120.5 (10)	O2—C1—C6	120.6 (16)	O1—C1—C6	120.3 (15)	C2—C1—O1	117.3 (3)
N1—C9—C8	114.8 (8)	O2—C1—C2	117.6 (16)	O2—C9—O1	116.1 (15)	C6—C1—O1	120.3 (3)
N1—C9—C10	122.1 (9)	O1—C9—O2	116.0 (16)	O2—C9—C8	126.2 (16)	O2—C9—O1	115.6 (3)
N3—C16—N2	123.3 (9)	O1—C9—C8	126.5 (18)	O1—C9—C8	117.6 (14)	O2—C9—C8	126.8 (3)
N3—C16—S1	116.1 (8)	O2—C9—C8	117.3 (16)	C11—C10—N1	114.9 (15)	O1—C9—C8	117.6 (3)
N2—C16—S1	120.5 (7)	C11—C10—N1	115.0 (15)	N1—C10—C8	117.5 (13)	C11—C10—N1	114.7 (3)
C17—C18—N3	113.8 (8)	N1—C10—C8	116.9 (14)	C10—C11—S1	111.3 (12)	N1—C10—C8	117.0 (3)
N3—C18—C19	116.4 (8)	C10—C11—S1	110.9 (14)	N1—C12—N2	123.8 (15)	C10—C11—S1	112.0 (2)
O1—C20—O2	116.3 (9)	N1—C12—N2	123.6 (16)	N1—C12—S1	116.5 (12)	N1—C12—N2	123.4 (3)
O1—C20—C19	126.5 (10)	N1—C12—S1	115.9 (13)	N2—C12—S1	119.6 (13)	N1—C12—S1	117.0 (2)
O2—C20—C19	117.2 (9)	N2—C12—S1	120.4 (13)	N3—C13—C23	121.9 (16)	N2—C12—S1	119.6 (2)
O2—C21—C27	116.9 (9)	N2—C13—C14	112.3 (15)	N3—C13—C14	113.57 (15)	N2—C13—C22	112.6 (2)
O2—C21—C22	121.7 (9)	N2—C13—C21	100.4 (13)	N2—C15—C16	113.0 (14)	N2—C13—C14	100.1 (2)
		C17—C18—O3	125.1 (2)	N2—C15—C14	100.4 (13)	N3—C15—C16	121.2 (3)
		O3—C18—C19	115.1 (2)	N1—C12—N2	123.8 (15)	N3—C15—C14	113.4 (3)
		N3—C22—C23	121.9 (17)	N1—C12—S1	116.5 (12)	C26—C25—O3	125.2 (3)
		N3—C22—C21	113.5 (15)	N2—C12—S1	119.6 (13)	O3—C25—C24	116.3 (4)
				N3—C13—C23	121.9 (16)		
				N3—C13—C14	113.5 (15)		

Table 5: Important X-ray bond angles (°) of compounds **1**-**4**, respectively (Atomic labels are with reference *ORTEP* plots Fig. 2).

1	Bond angle	**2**	Bond angle	**3**	Bond angle	**4**	Bond angle
C17—S1—C16	87.7	C11—S1—C12	87.8	C11—S1—C12	87.7	C11—S1—C12	87.7
C21—O2—C20	123.5	C1—O2—C9	123.5	C9—O1—C1	123.5	C9—O1—C1	123.5
C9—N1—N2	109.3	C18—O3—C20	118.0	C12—N1—C10	110.6	C25—O3—C28	118.2
C16—N2—N1	119.1	C12—N1—C10	110.8	C12—N2—N3	119.5	C12—N1—C10	110.5
C16—N2—C7	122.7	C12—N2—N3	119.7	C12—N2—C15	123.3	C12—N2—N3	119.5
N1—N2—C7	113.5	C12—N2—C13	122.5	N3—N2—C15	113.8	C12—N2—C13	123.6
C16—N3—C18	110.5	N3—N2—C13	113.6	C13—N3—N2	109.3	N3—N2—C13	113.9
C6—C1—Br1	119.1	C22—N3—N2	109.3	O1—C1—C2	117.6	C15—N3—N2	109.4
C2—C1—Br1	119.1	O2—C1—C6	120.6	O1—C1—C6	120.6	C2—C1—O1	117.6
N1—C9—C8	112.8	O2—C1—C2	117.7	O2—C9—O1	116.5	C6—C1—O1	120.6
N1—C9—C10	122.2	O1—C9—O2	116.7	O2—C9—C8	126.7	O2—C9—O1	116.5
N3—C16—N2	123.1	O1—C9—C8	126.7	O1—C9—C8	116.6	O2—C9—C8	126.8
N3—C16—S1	115.6	O2—C9—C8	116.5	C11—C10—N1	115.2	O1—C9—C8	116.6
N2—C16—S1	121.1	C11—C10—N1	115.2	N1—C10—C8	117.4	C11—C10—N1	115.3
C17—C18—N3	115.2	N1—C10—C8	116.9	C10—C11—S1	110.1	N1—C10—C8	117.4
N3—C18—C19	117.3	C10—C11—S1	110.6	N1—C12—N2	123.2	C10—C11—S1	110.7
O1—C20—O2	116.2	N1—C12—N2	122.6	N1—C12—S1	115.5	N1—C12—N2	123.4
O1—C20—C19	126.7	N1—C12—S1	115.4	N2—C12—S1	121.1	N1—C12—S1	115.5
O2—C20—C19	116.6	N2—C12—S1	121.8	N3—C13—C23	122.1	N2—C12—S1	121.0
O2—C21—C27	117.6	N2—C13—C14	113.1	N3—C13—C14	112.8	N2—C13—C22	113.2
O2—C21—C22	120.7	N2—C13—C21	100.6	N2—C15—C16	113.3	N2—C13—C14	100.5
		C17—C18—O3	124.6	N2—C15—C14	100.6	N3—C15—C16	122.1
		O3—C18—C19	115.4	N1—C12—N2	123.2	N3—C15—C14	112.8
		N3—C22—C23	122.1	N1—C12—S1	115.5	C26—C25—O3	124.7
		N3—C22—C21	112.8	N2—C12—S1	121.1	O3—C25—C24	115.6

Table 6: Important experimental and simulated vibrations (cm^{-1}) of compounds **1**-**4**.

1 (Calc.)	**1** (Exp.)	Assignment	**2** (Calc.)	**2** (Exp.)	Assignment	**3** (Calc.)	**3** (Exp.)	Assignment	**4** (Calc.)	**4** (Exp.)	Assignment
3089	3123	$\upsilon_s CH_{arom.}$	3089	3145	$\upsilon_s CH_{arom.}$	3089	3141	$\upsilon_s CH_{arom.}$	3089	3153	$\upsilon_s CH_{arom.}$
3080	---	υ_{as} $CH_{arom.}$	3080	---	$\upsilon_{as} CH_{arom.}$	3080	---	$\upsilon_{as} CH_{arom.}$	3080	---	$\upsilon_{as} CH_{arom.}$
1748	1709	$\upsilon_s C=O$	2967	---	$\upsilon_{as} CH_3$	1748	1718	$\upsilon_s C=O$	1748	1712	$\upsilon_s C=O$
1600	1606	$\upsilon_s C=C_{arom.}$	2906	---	$\upsilon_s CH_3$	1553	1550	$\upsilon_s C=C_{arom.}$	1610	1604	$\upsilon_s C=C_{arom.}$
1567	---	$\upsilon_s C=C_{arom.}$	1748	---	$\upsilon_s C=O$			$\upsilon_{as} C=N$	1554	1552	$\upsilon_s C=C_{arom.}$
1553	1545	$\upsilon_{as} C=N$	1606	1705	$\upsilon_{as} C=C_{arom.}$	1548	---	$\upsilon_s C=C_{arom.}$			$\upsilon_{as} C=N$
1545	1485	$\beta CH_{arom.}$	1554	1603	$\upsilon_s C=N$			$\upsilon_s C=N$	1548	1512	$\upsilon_{as} C=C_{arom.}$
1470	1443	$\beta CH_{arom.}$	1547	1554	$\upsilon_{as} C=N$	1372	1390	$\upsilon_s C=N$,			$\upsilon_s C=N$
1434	---	ρCH_2	1479	1487	$\beta CH_{arom.}$			βCH_2	1502	---	$\beta CH_{arom.}$
1371	1316	$\upsilon_s C=N$	1374	1380	$\upsilon_s C=N$	1301	---	$\upsilon_{as} C=C_{arom.}$	1372	---	$\upsilon_s C=N$
1282	1247	$\upsilon_s C=N$, $\beta CH_{arom.}$	1302	1317	$\upsilon_{as} C=C_{arom.}$ $\upsilon_s C$-N	1282 1162	1249 1174	$\beta CH_{arom.}$ $\beta CH_{arom.}$,	1348 1282	1330 ---	βCH $\beta CH_{arom.}$
1254	---	$\beta CH_{arom.}$	1282	1265	βCH_2,			ωCH_2	1246	1242	$\upsilon_s O$-Ph
1163	1172	$\beta CH_{arom.}$, $\omega CH_{arom.}$	1256	---	$\upsilon_{as} C=C_{arom.}$ $\beta CH_{arom.}$	1114 1069	1134 1043	$\upsilon_s N$-N $\upsilon_s O$-CH	1115 1069	1118 1027	$\upsilon_s N$-N $\upsilon_s O$-CH
1110	1132	$\upsilon_s N$-N	1251	---	$\upsilon_s O$-Ph	985	1005	$\upsilon_s O$-CH	984	1004	$\upsilon_s O$-CH
1068	1087	$\upsilon_s O$-CH	1164	---	$\beta CH_{arom.}$	752	752	$\upsilon_{as} S$-CH	751	754	$\upsilon_{as} S$-CH
984	962	$\upsilon_s O$-CH			ωCH_2						
955	---	γCH_2	1112	1134	$\upsilon_s N$-N						
752	752	$\upsilon_{as} S$-CH	1068	1053	$\upsilon_s O$-CH						
			1046	1010	$\upsilon_s O$-CH_3						
			751	751	$\upsilon_{as} S$-CH						

υ_s, Symmetric treching; **υ_{as}**, Asymmetric streching; **β**, In plane bending; **γ**, Out of plane bending; **ρ**, Scissoring; ω, In plane rotation

Table 7: AChE inhibition potential of all compounds (**1**-**4**).

S. No.	**IC_{50} (µM)**
Compound 1	70.94
Compound 2	3461.43
Compound 3	27.29
Compound 4	51113
Galantamine	44.02

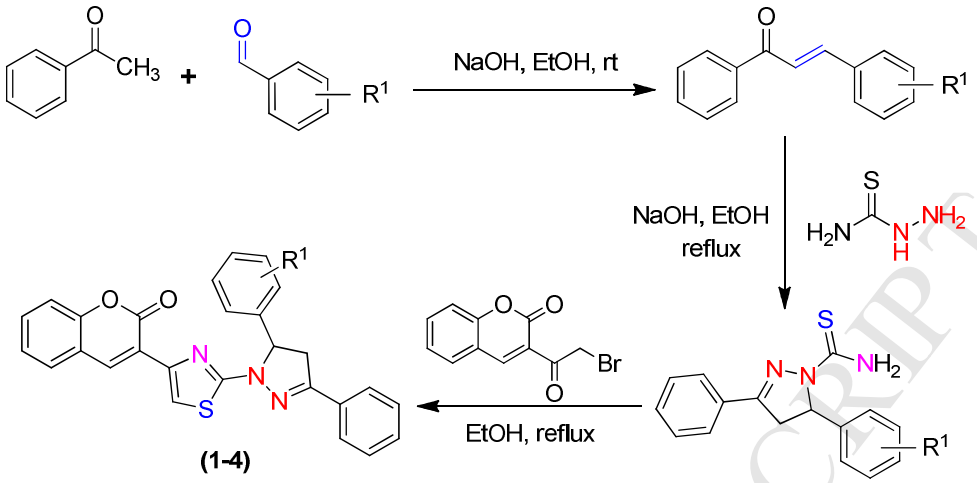

1) R^1 = 3BrPh **2)** R^1 = 3MeOPh **3)** R^1 = 4MePh **4)** R^1 = 4MeOPh

Figure 1

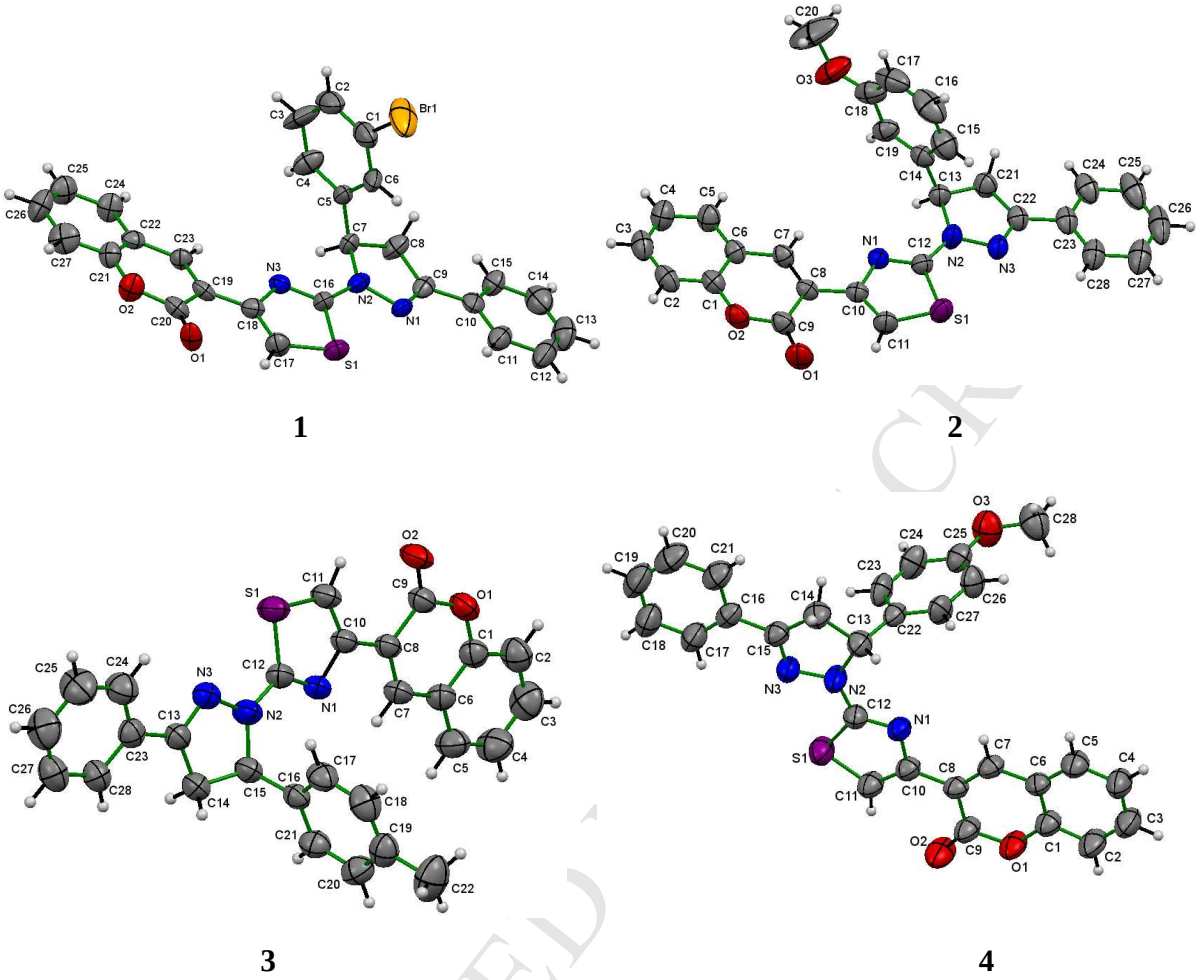

Figure 2

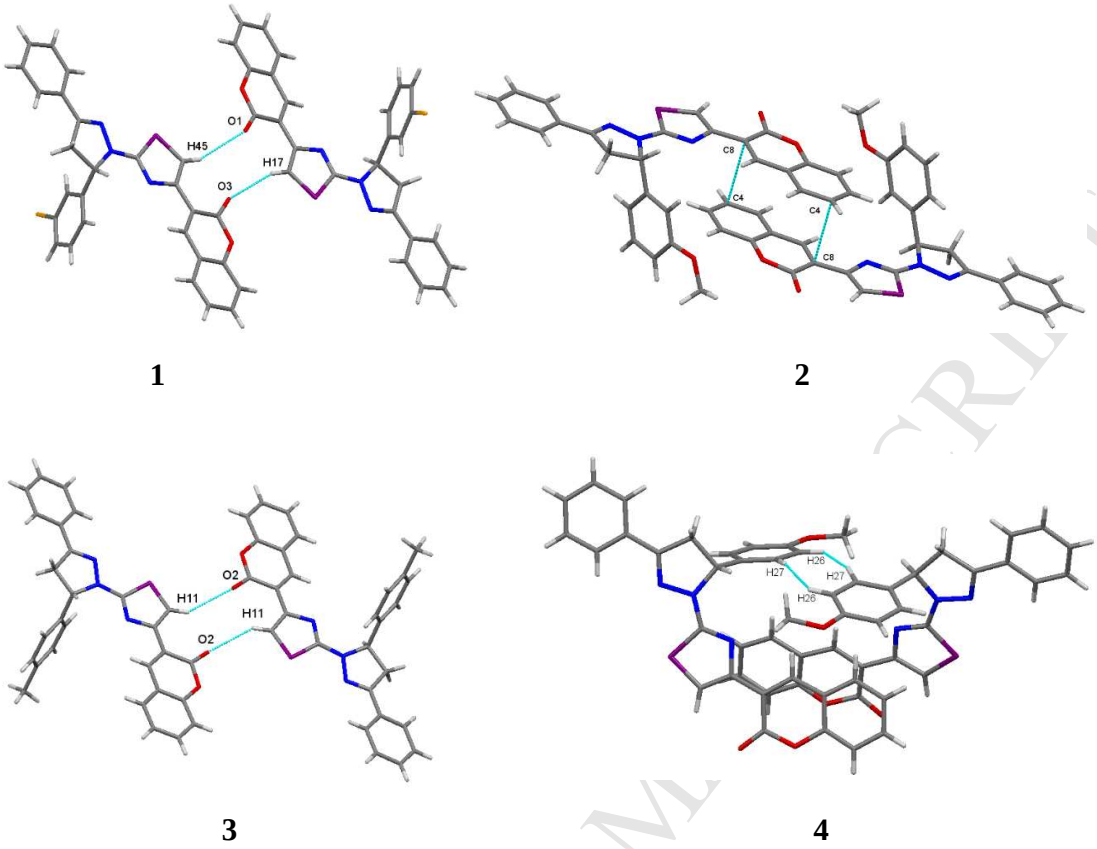

1 **2**

3 **4**

Figure 3

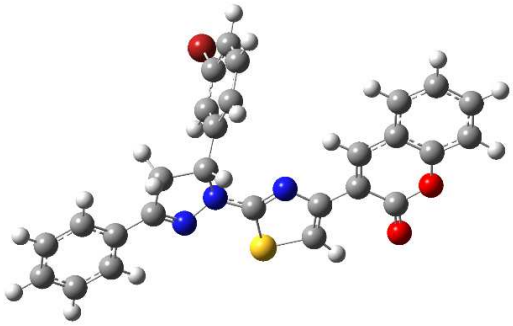

1

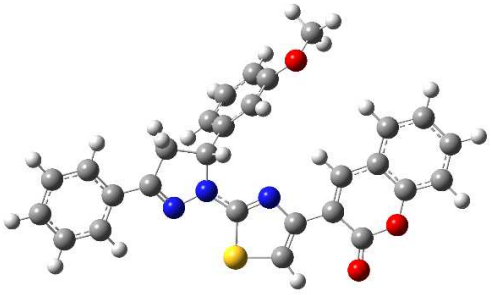

2

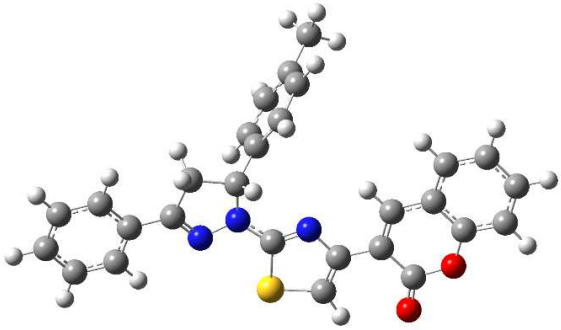

3

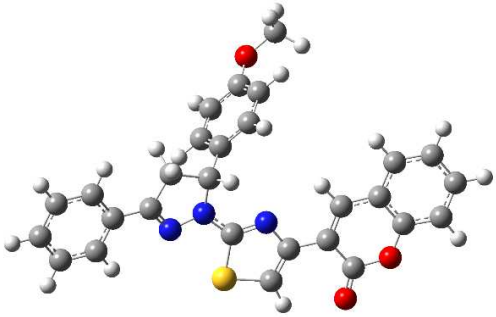

4

Figure 4

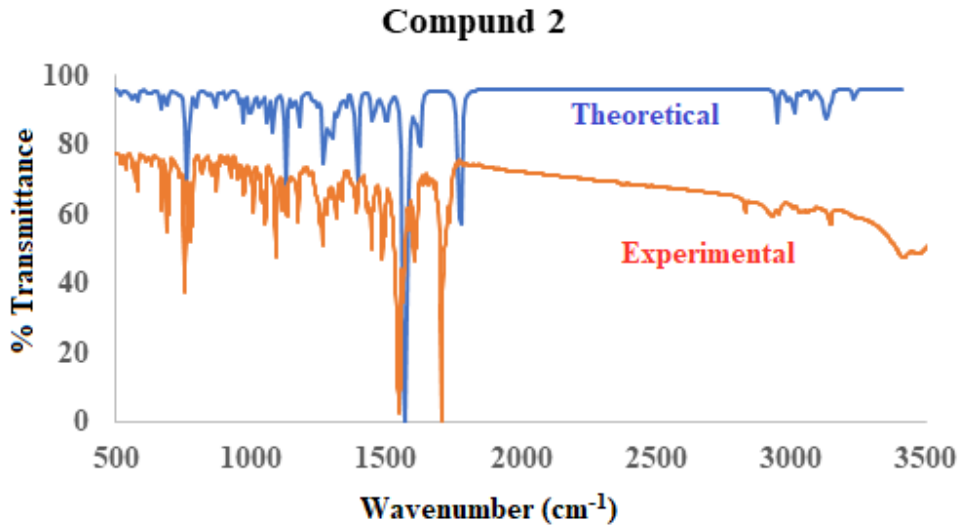

Figure. 5

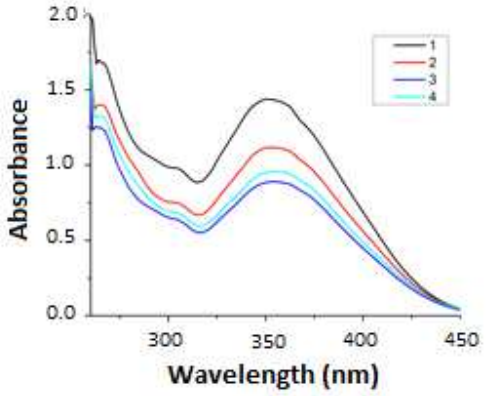

Experimental

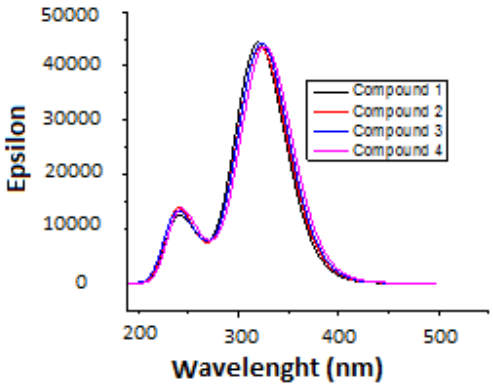

Theoretical

Figure 6

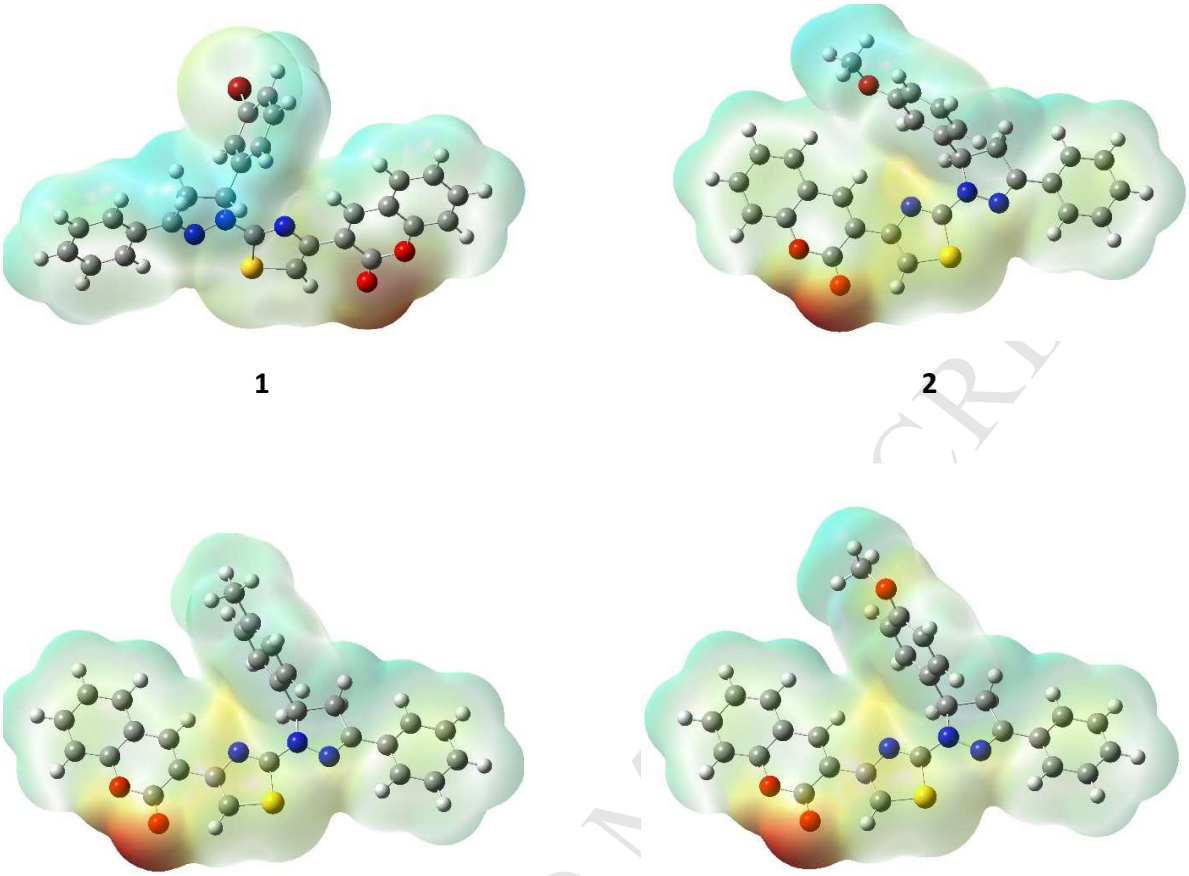

1 **2**

3 **4**

Figure 7

a)

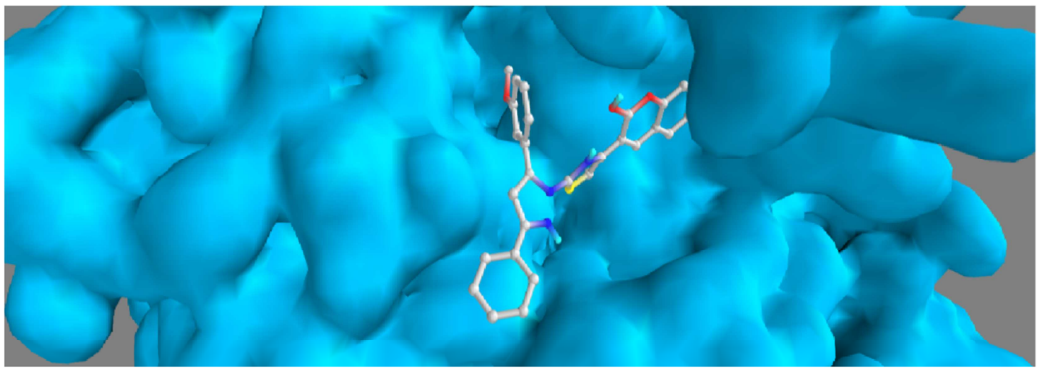

b)

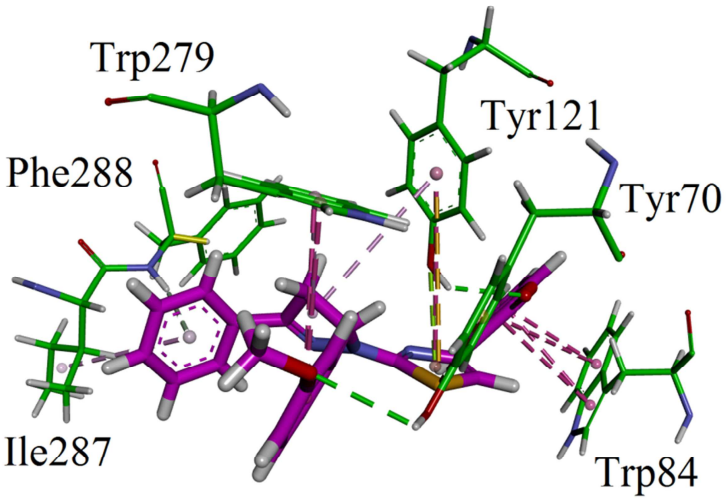

Figure 8

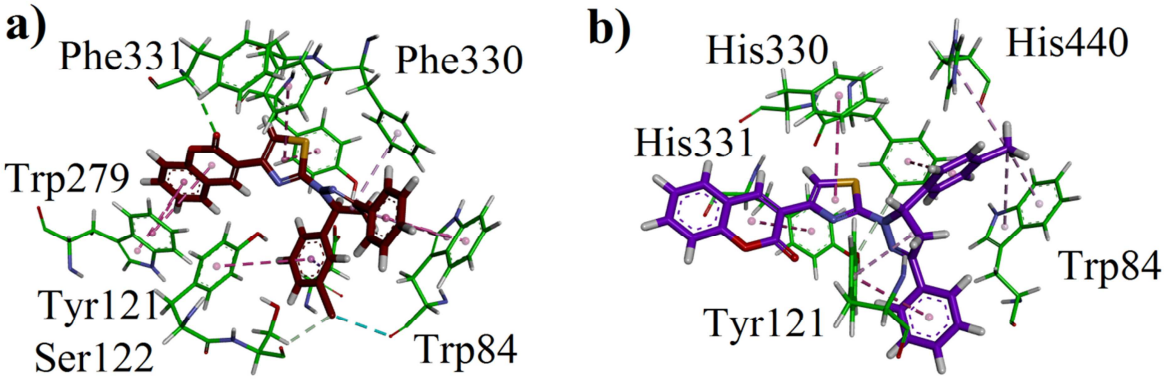

Figure 9

(i) Four new *3-(2-(3-Phenyl-5-substituted phenyl-4,5-dihydropyrazol-1-yl)thiazol-4-yl)-2H-chromen-2-one* derivatives have been synthesized.

(ii) Spectroscopic as well as X-ray data are compared by quantum chemical studies.

(iii) Enzyme inhibition potential of all compounds is tested against acetyl cholinesterase.

(iv) Molecular docking studies are executed with the help of AutoDock 4.2 and *Tc*AChE as target.